

SB7: the new bending-magnet double-headed dragon beamline at SuperACO

Fausto Sirotti,^{a*} Francois Polack,^a Jean Louis Cantin,^a Maurizio Sacchi,^a Renaud Delaunay,^a Michael Meyer^a and Marco Liberati^b

^aLaboratoire pour l'Utilisation du Rayonnement Electromagnetique, CNRS, CEA, MESR, BP 34, F-91485 Orsay, France, and ^bINFM – APE Project, Dipartimento di Fisica, Università di Modena, via Campi 213/a, 41100 Modena, Italy. E-mail: sirotti@lure.u-psud.fr

(Received 23 April 1999; accepted 18 October 1999)

A new beamline is now operational at LURE on bending-magnet 7 of the SuperACO storage ring in Orsay. The monochromator is of the 'dragon' type, designed to work in the energy range 150–1500 eV, and is equipped with a double vertical focusing mirror in order to allow for fast switching of light polarization. In this paper the results of photoion-yield experiments performed on N₂, Ar and Ne gases are presented. The observed resonance structures enable us to determine the available energy resolution: a resolving power higher than 8500 is obtained at the Ar 2*p*, N 1*s* and Ne *K*-edges when using all the optical elements at full aperture. The total flux as a function of the measured photon energy resolution and the characterization of the double-head behaviour in delivering circularly polarized light are reported.

Keywords: soft X-ray beamlines; circular polarization.

1. Introduction

The project for the construction of the SB7 beamline on the storage ring SuperACO (LURE, Orsay) started in early 1996 following a few basic ideas on the desired performances and possible applications:

- (i) Wide energy range (100–1500 eV) centred around the SuperACO critical energy (666 eV).
- (ii) Smooth variation of the intensity over this range to perform photon-energy-dependent spectroscopic studies.
- (iii) Tunable photon polarization, with the possibility of fast switching from one helicity state to the other.
- (iv) A reasonable intensity ($\sim 10^9$ photons s⁻¹ on the sample) and energy resolution ($>5 \times 10^3$ resolving power) for routine absorption and photoemission experiments.

To match all these requirements the choice was directed to a beamline with an optical layout similar to that of the 'double-headed' dragon monochromator (Chen & Sette, 1989; Chen, 1992), mounted on a bending-magnet source. The bending magnet provides linearly polarized light as well as elliptically polarized light of both helicities, and the use of grazing-incidence optics preserves the degree of polarization of the light.

2. Beamline description

The characteristics of the relevant optical elements (summarized in Table 1) are as follows (see Fig. 1).

An elliptical mirror M1 focuses the beam horizontally in the region between the gratings and the exit slit. Its large

horizontal acceptance (15 mrad) allows a high flux to be obtained, even using a bending magnet.

Two spherical mirrors M2' and M2'' (each one accepting 7 mrad of horizontal angle) focus the beam vertically onto the entrance slit. The two mirrors can be displaced vertically and rotated in order to intercept the incoming photons at different heights with respect to the orbit plane and still deviate the reflected beams along the same optical path. As a result, photons of positive (above plane) and negative (below plane) helicity can be separated horizontally and directed onto the sample at the same time and with the same energy.

A slit P is placed after the vertical focusing mirrors in order to define the degree of polarization of the two beams along the same optical path.

A chopper is placed before the entrance slit and selects the polarized beam that reaches the monochromator. It is composed of a rotating disc whose diameter is 330 mm and which presents three concentric holes arrangements in order to allow the modulation of the transmitted light. It can work in step mode, alternating left and right polarizations, or in continuous mode combined with a lock-in detection. The chopper is connected to the beamline with long bellows and stands independent from the concrete support of the beamline in order to reduce the propagation of mechanical vibrations to the optical elements.

The monochromator consists of a fixed entrance slit S1 (minimum aperture 5 μ m), a set of four spherical gratings (SGM) which can be interchanged under vacuum, and a movable exit slit S2. The grating radius of curvature was

Table 1

Characteristics of the optical elements of the SB7 beamline.

All the optics are platinum coated.

Horizontal focusing mirror	
Material	Ultra low expansion glass
Shape	Elliptical
Radius of curvature	90.8 m
Source distance	3.6 m
Focus distance	7 m
Incidence	87°
Useful area	1000 mm × 20 mm
Vertical focusing mirrors	
Material	Silica
Shape	Spherical
Radius of curvature	111.670 mm
Useful area	245 mm × 22 mm
Slope error	<1.2 μrad
Spherical gratings	
Material	Silica
Shape	Spherical
Radius of curvature	71.400 mm
Useful area	175 mm × 15 mm
Slope error	<1.1 μrad
Lines mm ⁻¹	500, 800, 1200, 1800
Toroidal focusing mirror	
Material	Zerodur
Shape	Toroidal
Radius of curvature	78.830 mm, 73.962 mm
Useful area	210 mm × 40 mm
Slope error	<10 μrad

chosen such that the defocus curve is approximately symmetrical throughout the scanning range. The slit travel is thus reduced to 400 mm.

A toroidal mirror M3 refocuses the monochromatic beam onto the sample position (spot size of 1 × 3 mm). All the beamline elements have been constructed by ISA, Jobin Yvon (Longjumeau, France) except the first horizontal focusing mirror (SESO, Grenoble, France).

An original feature of the SB7 beamline is the astigmatic optical design with independent focusing in the vertical and horizontal planes. As a matter of fact only vertical focusing, in the dispersion plane, is required inside the mono-

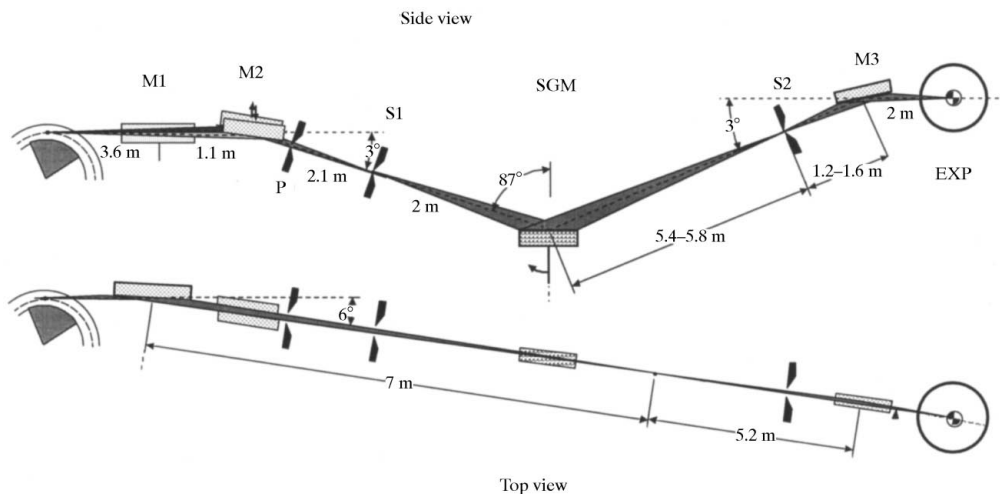
chromator, between the entrance and exit slit. To improve the slit-to-slit imaging properties of the monochromator it is better to position any horizontally focusing element outside the monochromator.

Vertical and horizontal focusing can be designed almost independently. The vertical focusing system needs three elements: a prefocusing mirror, the spherical grating and a postfocusing mirror. The vertical magnification of the prefocus system is chosen to be ~2 (2.24) as a compromise between obtaining a narrow line image of the source on the slit (aberration), filling the SGM aperture angle and optics length. The vertical magnification of the postfocusing system, for equivalent reasons, can be chosen to be ~1/2.5 because the exit slit is always narrow, and this configuration tolerates a large change in slit position.

In the horizontal plane the two horizontal focusing optics must be matched to produce a small spot image of the source on the sample. The intermediate focus point (real or virtual) can be chosen to obtain any desired magnification. It was set near the middle of the monochromator because it reduces the beam footprint on the grating and it allows a reasonable slit length to be maintained, 30 mm for both entrance and exit slit. The total magnification ratio is 0.75. It has been chosen to combine the horizontal and vertical postfocusing into one toroidal mirror. This scheme contributes to reducing the overall length of the beamline. On the contrary, the accuracy requirement and the double-head prefocusing system have imposed separate horizontal and vertical focusing mirrors.

Fig. 2 reports the best resolving power ($S1 = 10 \mu\text{m}$) calculated (Delcamp *et al.*, 1998) for this beamline showing that the required value of 10^4 can be reached up to a photon energy of 800 eV, and that at 1400 eV an excellent value of 5000 can still be obtained. The solid symbols shown in the figure represent the measured resolving power evaluated as explained in the following.

Beyond the choice of the optical layout we paid particular attention to the problem of mechanical stability and

**Figure 1**

Optical layout of the SB7 beamline at SuperACO. EXP = experimental chamber.

coupling to the floor vibrations in the SuperACO experimental hall. Based on previous experience (Delcamp *et al.*, 1996) it was decided from the beginning that the entire beamline should stand on a single concrete beam, decoupled from the floor.

Fig. 3 shows the concrete stand supporting the optical elements of the beamline (with the exception of M3): the optical elements are mounted on the upper beam, which stands on concrete piles driven through the floor to a second concrete platform built on firm ground. A dedicated study dealt with the frequency analysis of the characteristic ground vibrations and their transmission through the concrete support (the attenuation coefficient is higher than that of steel). The results, based on finite-elements model calculations, indicated that the maximum displacements and rotations induced on the optical elements are at least ten times smaller than the required tolerances. With the help of these simulations the concrete support structure was designed in order that it does not amplify any frequency over 30 Hz (LURE report, unpublished).

In order to maintain the long-term stability of the alignment, the upper concrete beam and the optical elements are thermalized to 303 K.

3. Photon energy resolution

Core-level resonances in the 150–1400 eV energy range, covered by the beamline, have natural widths larger than the ultimate resolution expected for this beamline. The experimental determination of the resolving power R is therefore strongly dependent on the natural line widths assumed in the deconvolution procedure. Over the last ten years the construction of new beamlines with better performances has induced a systematic reduction of the published natural line-width values, clearly indicating that absolute values of R should be taken with care.

Therefore, in the following, the measured line shapes will be reported along with their total width obtained using a simple Lorentzian line shape. The values of Gaussian broadening and of resolving power are determined by using

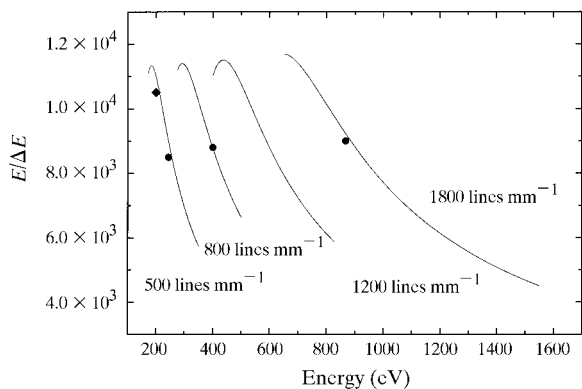


Figure 2 SB7 monochromator resolving power for each grating calculated for an entrance slit of 10 μm . The points represent the resolving power values measured as explained in the text.

Voigt functions in the fitting procedure and by fixing the natural widths to the smallest value found in the literature.

The resolution tests were performed measuring the ion yield spectra in the energy region close to the resonant $2p$ excitation of atomic argon as well as the $1s$ excitation of molecular nitrogen and atomic neon. The spectra were obtained by monitoring the total number of ions produced in the interaction region between the monochromatic synchrotron radiation beam and an effusive gas jet emanating from a small nozzle. The experiments were performed with a total gas pressure in the experimental chamber ranging from 5×10^{-5} to 2×10^{-4} Pa without any separating window between the ionization region and the beamline. The photon flux impinging on the sample was measured with a calibrated GaAsP photodiode installed in the experimental chamber behind the ionization region.

All the resolution tests were performed using all the optical elements at full aperture. The spectrum of the Ar $L_{2,3}$ excitations is shown in Fig. 4 as measured with the 500 lines mm^{-1} grating.

The two Ar* $2p \rightarrow nd$ Rydberg series converging to the Ar* $2p^5\ ^2P_{3/2}$ and $\ ^2P_{1/2}$ thresholds are clearly resolved up to the $n = 7$ levels. For the total width of the Ar* $2p^5$ ($\ ^2P_{3/2}$) $4s$

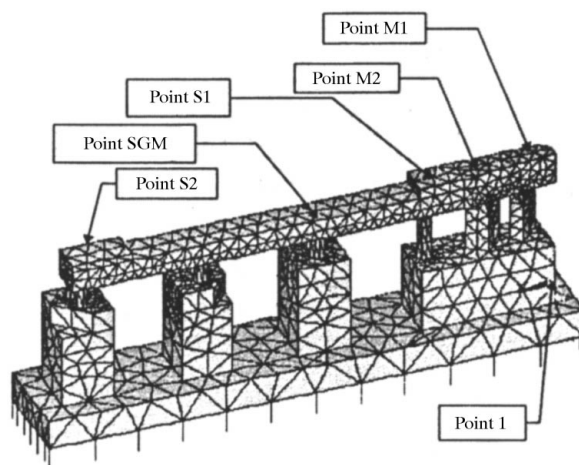


Figure 3 Schematic diagram of the concrete support of the beamline. The positions of the optical elements are indicated.

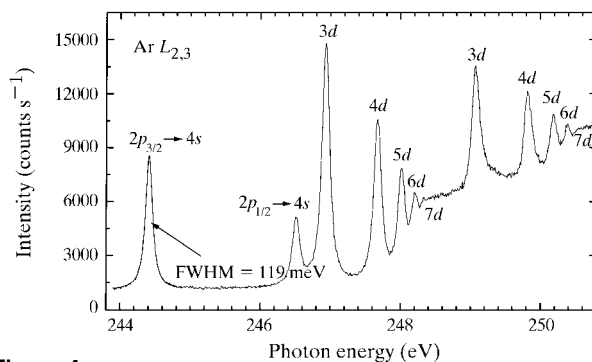


Figure 4 Argon $L_{2,3}$ excitations. The total Lorentzian width of the $2p_{3/2} \rightarrow 4s$ transition is 119 meV.

resonance at $h\nu = 244.4$ eV a value of $\Gamma_{\text{total}} = 119$ meV was determined using a fit of a single Lorentzian profile. Assuming a contribution from the natural line width of $\Gamma_{\text{nat}} = 114$ meV (Sairanen *et al.*, 1996; Prince *et al.*, 1998) we obtain an experimental (Gaussian) FWHM of 29 meV corresponding to a resolving power $E/\Delta E$ of ~ 8500 in the considered photon energy region.

In Fig. 5 the wide-range K -shell photoion-yield spectrum of N_2 is displayed. The region around the $\text{N } 1s \rightarrow 1\pi_g^*$ resonant excitation and the high-energy region (405 eV $\leq h\nu \leq 425$ eV) were recorded with gas pressures of $p(\text{N}_2) = 1.2 \times 10^{-4}$ Pa and 5.7×10^{-4} Pa, respectively, resulting in an approximately five times larger counting rate in the high-energy region. All structures measured in photoabsorption at the first dragon beamline (Chen *et al.*, 1989) are also present in the spectrum of Fig. 5. In particular, the small structures around $h\nu = 414.5$ eV, which arise from resonant double excitations, are clearly observed, and in the $\text{N } 1s \rightarrow \text{Rydberg}$ transitions the small structure

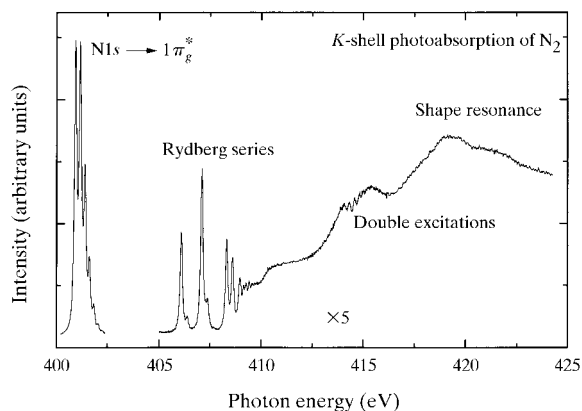


Figure 5
 K -shell photoexcitation spectrum of N_2 .

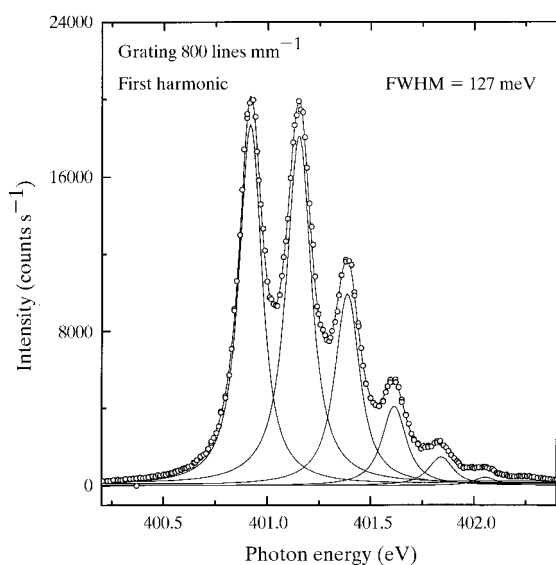


Figure 6
Vibrational levels of the $\text{N}_2 1s \rightarrow \pi^*$ transition measured at the first order with the 1200 lines mm^{-1} grating. The solid line is the best fit obtained with six Voigt functions.

attributed to the $7p\pi$ Rydberg state [labelled No. 14 in Chen *et al.* (1989)] could be resolved.

The photoexcitation of the $(1s^{-1}\pi^*)$ resonance in nitrogen has become the standard resolution test for new monochromators in this energy range. A high-resolution ion-yield spectrum, measured with the 800 lines mm^{-1} grating and entrance-slit openings as well as exit-slit openings of ~ 5 μm , is presented in Fig. 6 showing the vibration modes of the $\text{N } 1s\pi^*$ resonance up to $\nu = 7$. The value r defined as the ratio between the intensities of the first minimum and the third peak ($\nu = 2$) is commonly used for a parameter-free comparison of monochromator resolution (Cvetko *et al.*, 1997; Quaresima *et al.*, 1995). For our first-order spectrum we obtain $r = 0.78$, whereas a value of $r = 0.72$ is obtained with the 500 lines mm^{-1} grating in second-order diffraction. The total full width at half-maximum (FWHM) of the first peak ($\nu = 0$) is determined

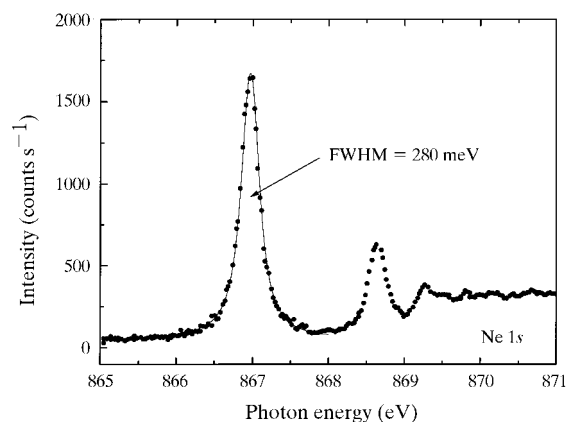


Figure 7
 $\text{Ne } K$ -edge spectrum measured with the 1800 lines mm^{-1} grating at the first order. The continuous line is the best fit obtained with a simple Lorentzian function.

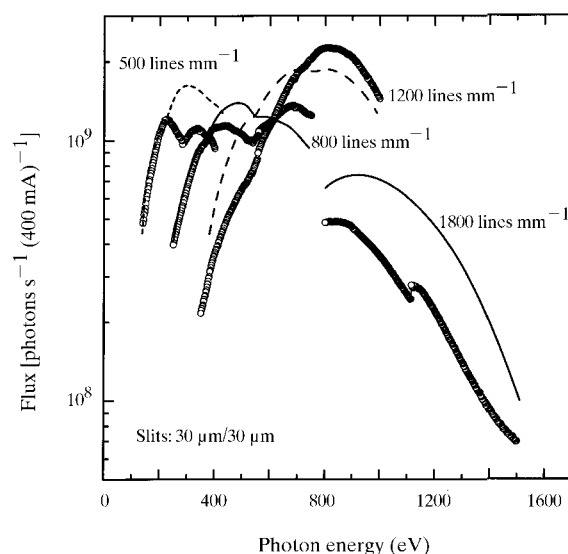


Figure 8
Experimental (symbols) and calculated (lines) photon flux on the sample as a function of the photon energy for the four gratings obtained using entrance and exit slits of 30 μm .

to be $\Gamma_{\text{total}} = 127$ meV, obtained using simple Lorentzian functions. As already mentioned above, the evaluation of the resolution depends strongly on the natural line width used in the fitting procedure. The spectrum in Fig. 6 is deconvoluted with six Voigt profiles whose Lorentzian width was fixed at $\Gamma_{\text{nat}} = 115$ meV (Prince *et al.*, 1998). The best-fit procedure results in a Gaussian width of 45 meV corresponding to a resolving power of $E/\Delta E = 8800$. The natural width of 115 meV was defined by considering a

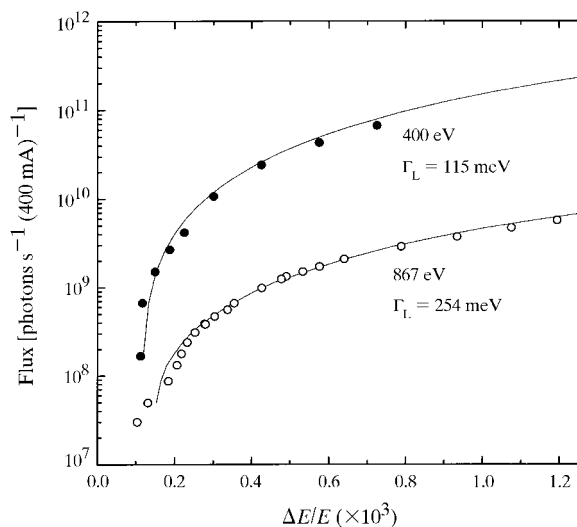


Figure 9
Measured flux at the N $1s \rightarrow \pi^*$ and Ne $1s \rightarrow 3p$ transitions as a function of the Gaussian broadening obtained for Lorentzian widths of 115 eV and 254 meV, respectively.

resolving power of ~ 20000 at the second order in Prince *et al.* (1998). The same fit procedure on the second harmonic of the 500 lines mm^{-1} grating yields a resolving power of 10500. Since the 200 eV radiation in the first and second order is along the same path and has the same dispersion factor, this resolving power also applies to 200 eV radiation.

Finally, the excitation spectrum near the Ne K -edge measured with the 1800 lines mm^{-1} grating is reported in Fig. 7 together with a Lorentzian function (solid line) describing the observed $1s \rightarrow 3p$ transition at $h\nu = 867$ eV. For the total width a value of $\Gamma_{\text{total}} = 280$ meV is obtained. The fitting procedure with a Voigt function whose Lorentzian width was fixed at $\Gamma_{\text{nat}} = 254$ meV provides an experimental broadening of 90 meV which corresponds to a resolving power of $E/\Delta E = 9500$. The natural width of 254 meV was defined by considering a resolving power of ~ 20000 at the second order (Prince *et al.*, 1998). The obtained resolving powers are compared with the calculated values in Fig. 2.

The photon flux transmitted by the beamline as a function of the photon energy is displayed in Fig. 8 (symbols) for a fixed aperture of the slits of 30 μm which corresponds to a resolving power of ~ 4000 . More than 10^9 photons s^{-1} are available in the energy range 200–1000 eV. The signatures of the carbon and the oxygen present on the optics are visible in the experimental curves of the 500 and 800 lines mm^{-1} gratings. The structure at ~ 1100 eV in the 1800 lines mm^{-1} grating transmission curve is due to the GaAs diode used for measuring the photon intensity. The

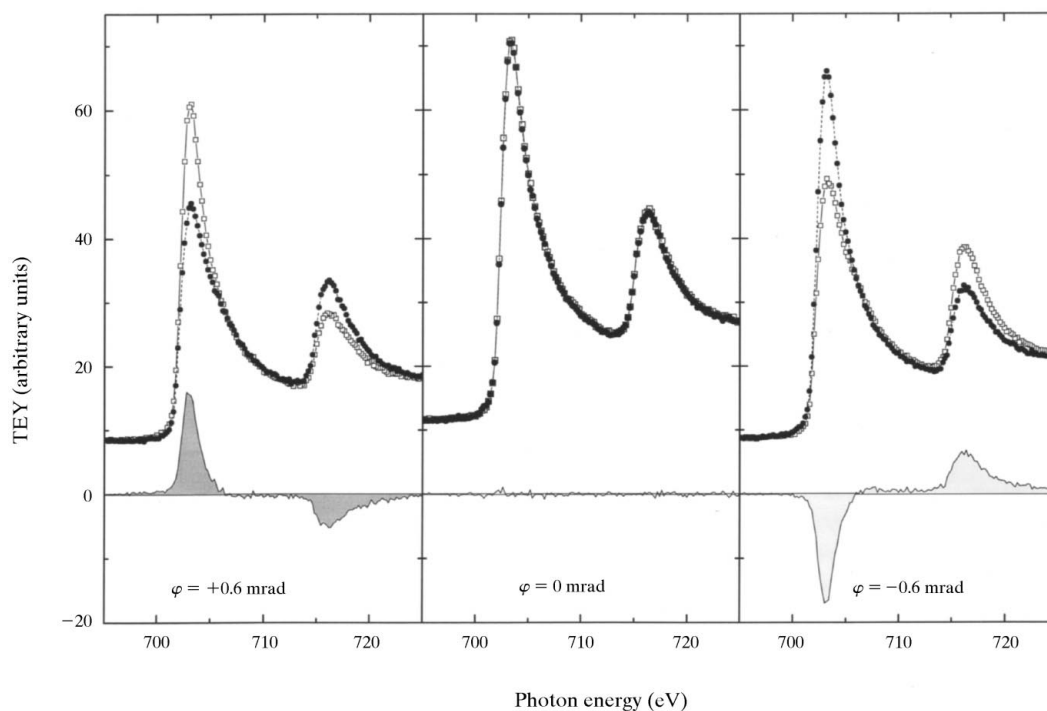


Figure 10
Fe $L_{2,3}$ photoabsorption spectra measured in total electrons yield (TEY) obtained by reversing the sample magnetization direction for three positions [above (left), in (centre) and below (right) the orbital plane] for one of the two vertical focusing mirrors. The corresponding difference spectra are shown at the bottom.

measured flux is compared with computed values (lines). They account for the source brightness, the geometrical aperture, surface reflectivities calculated from Henke's optical data tables (Henke *et al.*, 1993), and grating diffraction efficiency computed with the electromagnetic code *CARPEM* (Mirone *et al.*, 1998). The calculated flux of Fig. 8 is divided by a factor of three. A source for this discrepancy can be found in the thermal deformation of the first optical element (M1) which is not cooled. Additional losses can be attributed to the finite accuracy of optimization and alignment procedure mainly concerning the focalization on the entrance slits.

The photon flux available on the sample, as well as the photon energy resolution, is of fundamental importance in order to evaluate the feasibility of a given experiment. Fig. 9 presents the relationship between the energy resolution and available flux, while the slits widths are varied. Experimental points for 400 eV light (1220 lines mm^{-1} grating) and 867 eV light (1800 lines mm^{-1}) are compared with the calculated values. The intensity was measured using the photodiode as a function of the slits openings (entrance = exit), and the corresponding Gaussian broadening was determined with a fitting procedure performed using Voigt functions whose Lorentzian width was fixed as described previously. The calculated energy resolution is obtained by adding quadratically the experimental Gaussian broadening for zero slit width to the theoretical broadening due to the slit width. The calculated flux is obtained by multiplying the measured flux with 30 mm slits by a relative acceptance factor. The latter accounts for the Gaussian illumination of the entrance slit and the bandpass selection of the exit slit.

4. Light polarization selection

Circularly polarized light is obtained when only a fraction of the beam emitted above or below the storage-ring plane is focused onto S1 and into the monochromator. The beam path is defined by the position and aperture of the slit P in Fig. 1. The selection of the polarization of the light is then defined by a combined rotation and translation of M2 that directs the photons of the desired polarization (above, in or below plane emission) along the beam path defined by P and S1. Since the two mirrors M2' and M2'' can be positioned independently, two beams of different polarization can be sent simultaneously into the monochromator. Their trajectories in the dispersive (vertical) plane are identical, and so are the photon energies obtained on the sample.

The sizes of the vertical focusing mirrors were calculated in order to intercept the synchrotron beam in the range from -2 to $+2$ mrad with respect to the orbital plane. For the polarization test experiments the P slit was set in order to define 0.2 mrad of vertical angular acceptance.

Light polarization tests were performed measuring the magnetic circular dichroism at the $L_{2,3}$ edges of iron on an FeNiB sample mounted to close the gap of a soft iron yoke.

The sample magnetization direction was set to an angle of 20° with respect to the light-propagation direction.

The difference spectra which can be recorded by reversing the sample magnetization are proportional to the circular polarization rate of the incoming beam multiplied by the total intensity. Fig. 10 shows the spectra obtained setting one of the two mirrors in the orbit plane (central panel) and at an angle of 0.6 mrad above (left panel) and below (right panel) the orbit plane. The curves with solid and open symbols in the figure correspond to the two magnetization directions on the sample, and the corresponding difference spectra are reported at the bottom. The orbital plane position was determined by setting the monochromator to the photon energy corresponding to the maximum of the difference signal in Fig. 10 and scanning the translation and rotation movements of the two vertical focusing mirrors. The total intensity measured as a function

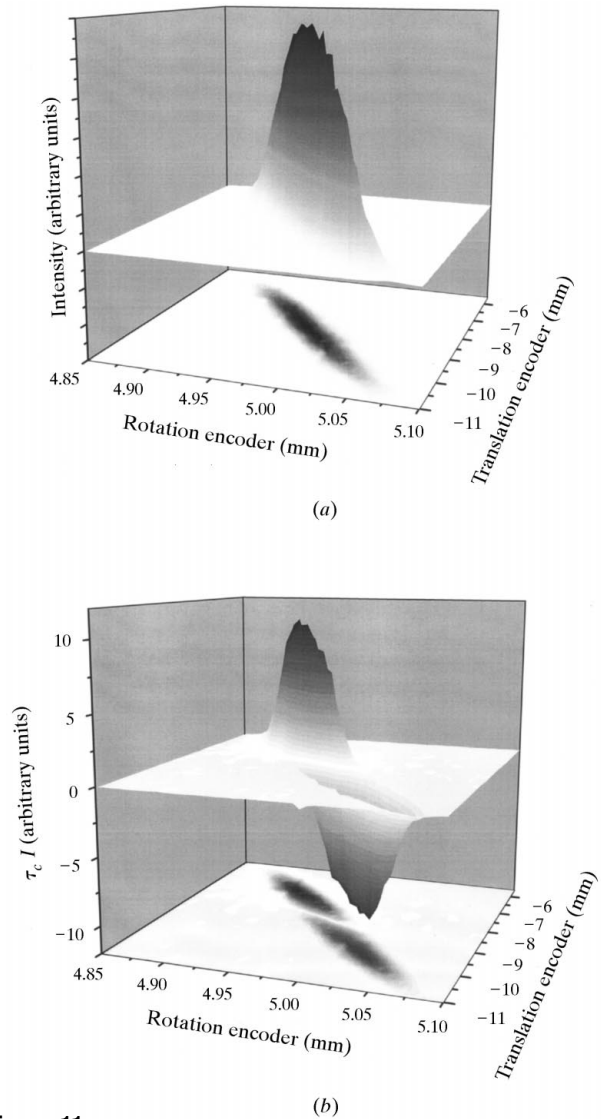


Figure 11 Total intensity (a) and intensity difference signal (b) recorded at a fixed photon energy as a function of the translation and rotation encoders of one of the two vertical focusing mirrors.

of the vertical focusing mirror translation and rotation encoders is reported in Fig. 11(a). The difference signal obtained for the two opposite magnetization directions is shown in Fig. 11(b). The sign reversal of the difference signal indicates the reversal of the circular polarization contribution of the selected beam.

Taking into account geometrical factors, the circular polarization rate for the spectra shown in Fig. 10 is evaluated to be about 80%.

The two beams can be selected with the chopper described above in order to obtain a fast polarization switch either in the step mode with a switching time less than 300 ms or in continuous mode with a maximum frequency of 800 Hz corresponding to a rotation speed of 1000 r.p.m.

5. Conclusions

The SB7 beamline was operational two years after from the start of the project. The resolving powers measured at the Ar $2p$, N $1s$ and Ne K -edges ranges between 8500 and 9500. The results obtained compare well with the expectations and predictions in terms of ultimate resolution and flux.

The double-head system for the determination of the light polarization was successfully tested and allows a fast switching of the photon helicity without affecting the photon energy scale. The UHV-compatible chopper for fast light polarization switching is under commissioning.

The photon flux available on the sample when the ultimate resolution is obtained will allow photoabsorption and

photoemission experiments to be easily performed on solid surfaces with linear and circular polarization of the light, spanning a wide energy range with only smooth variation of the intensity.

References

- Chen, C. T. (1992). *Rev. Sci. Instrum.* **63**, 1229–1333.
- Chen, C. T., Ma, Y. & Sette, F. (1989). *Phys. Rev. A*, **40**, 6737–6740.
- Chen, C. T. & Sette, F. (1989). *Rev. Sci. Instrum.* **60**, 1616–1621.
- Cvetko, D., Floreano, L., Gotter, R., Malvezzi, M., Marassi, L., Morgante, A., Naletto, G., Santaniello, A., Stefani, G., Tommasini, F., Todello, G. & Verdini, A. (1997). *Proc. SPIE*, **3150**, 86–96.
- Delcamp, E., Lagarde, B. & Polack, F. (1996). LURE Internal Report. Unpublished.
- Delcamp, E., Lagarde, B. & Polack, F. (1998). *Proc. SPIE*, **2856**, 120–128.
- Henke, B. L., Gullikson, E. M. & Davis, J. C. (1993). *Atom. Data Nucl. Data Tables*, **54**, 181–342.
- Mirone, A., Delcamp, E., Idir, M., Cauchon, G., Bizeuil, C., Polack, F. & Dhez, P. (1998). *Appl. Opt.* **37**, 5816–5822.
- Prince, K. C., Blyth, R. R., Delaunay, R., Zitnik, M., Krempasky, J., Slezak, J., Camilloni, R., Avaldi, L., Coreno, M., Stefani, G., Furlani, C., de Simone, M. & Stranges, S. (1998). *J. Synchrotron Rad.* **5**, 565–568.
- Quaresima, C., Ottaviani, C., Matteucci, M., Crotti, C., Antonini, A., Capozzi, M., Rinaldi, S., Luce, M., Perfetti, P., Prince, K. C., Astaldi, C., Zacchigna, M., Romanzin, L. & Savoia, A. (1995). *Nucl. Instrum. Methods*, **A364**, 374–379.
- Sairanen, O. P., Kivimäki, A., Nömmiste, E., Askela, H. & Askela, S. (1996). *Phys. Rev. A*, **54**, 2834–2839.